Identification the Shape of Biconcave Red Blood Cells Using Histogram of Oriented Gradients and Covariance Features

G. Apostolopoulos, *Member, IEEE,* S.V. Tsinopoulos, and E. Dermatas

***Abstract*—In this paper, a novel methodology for estimating the shape of human biconcave Red Blood Cells (RBCs), using color scattering images, is presented. The information retrieval process includes, image normalization, features extraction using both Histogram of Oriented Gradients (HoG) and region covariance features (RCoV); and features dimensionality reduction using the Independent Component Analysis (ICA). The points of interest (PoIs) are detected using the Harris-corner detector in order to extract the image features. A scheme using adjustable algorithms, i.e. support vectors machine (SVM) is adopted in order to fuse the multimodal features. A Radial Basis Function Neural Network (RBF-NN) estimates the RBC geometrical properties. The proposed method is evaluated in both regression and identification tasks by processing images of a simulated device used to acquire scattering phenomena of moving RBCs. The evaluation database includes 23625 scattering images, obtained by means of the Boundary Element Method. The regression and identification accuracy of the actual RBC shape is estimated using three feature sets in the presence of additive white Gaussian noise from 60 to 10 dB SNR, giving a mean error rate less than 1 percent of the actual RBC shape, and more than 99 percent mean identification rate in a set of valid RBCs size.**

I. Introduction

Red blood cells (RBCs) are the most common type of blood cell, filled with hemoglobin, a bio-molecule that can bind to oxygen. Several blood diseases change the typical size and distribution of red blood cells. Light scattering has been used for efficient and accurate measurement of the geometrical properties of micro-particles [1-3]. Real scattering images are obtained using devices given in [4-11]. A new low-cost device (Fig. 1) [12] for acquisition of scattering images of biconcave-shaped RBCs has already been proposed, where digital images are derived when a LED beam illuminates the RBCs-flow at different positions of the color filter wheel. The device is used to estimate the diameter, maximum and the minimum thickness of the human RBCs and to identify the RBCs geometrical properties using image processing and non-linear regression techniques. According to the linear theory of light, the acquisition of multiple images for the same RBC solution using the low-cost but broad spectrum LEDs and color filters produces rich but also redundant information, related to wavelength-dependent absorption and scattering phenomena.

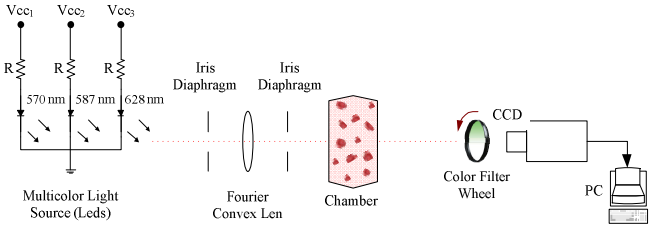

Fig. 1. The schematic diagram of the device used to acquire scattering images in a RBC-flow according to [12].

Therefore, in the neural-network based estimator and identification system of the RBC geometric properties, noise, data reduction and robust feature extraction are implemented, preserving and compress the scattering information.

In this work, we employ both Histogram of Oriented Gradients (HoG) and Region Covariance (RCoV) features, extracted from all locations of a grid on the scattering image, as candidates of the primitive feature vector. Support Vector Machines (SVM) is applied to primitive feature vector to fuse the multimodal features. Since HoG features extracted from regions without edges are not effective for classification we use points of interest (PoIs) to gather training samples only from effective regions of the scattering image. The PoIs are salient image patches that contain rich local information about the scattering image. A great variety of approaches have been developed for the purpose of detecting and extracting the PoIs [13-15]. In this paper the fast, robust and rotation invariant, Harris detector is used to detect the PoIs.

The structure of this paper is as follows: Section 2 presents the feature extraction, the feature dimension reduction, the feature fusion process and the proposed neural regression and identification methods. The evaluation process including the numerical experiments, the regression and identification results are presented and discussed in section 3. A short conclusion is given in the last section.

II. RBC Shape Estimation

According to [16,17], healthy human RBCs (Fig. 2) have an axisymmetric biconcave-shaped geometry with z indicating the axis of the symmetry. Typical values of the important parameters: diameter R_1, the maximum thickness

Manuscript received July 12, 2013.

G. Apostolopoulos is with the Electrical Engineering and Computer Technology Department, University of Patras, 6 Eratosthenous Str, 26500, Patras, Greece (corresponding author to provide phone: +30-2610-991722; fax: +30-2610-991855; e-mail: gapost@george.wcl2.ee.upatras.gr).

S.V. Tsinopoulos, is with Mechanical Engineering Department, Technological Educational Institute of Western Greece, 1 Megalou Alexandrou Str, Patras, Greece (e-mail: stsinop@teipat.gr).

E. Dermatas is with the Electrical Engineering and Computer Technology Department, University of Patras, 6 Eratosthenous Str, 26500, Patras, Greece, (e-mail: dermatas@george.wcl2.ee.upatras.gr).

978-1-4799-3163-7/13/$31.00 ©2013 IEEE

R_2 and the ratio $\frac{R_3}{R_2}$ of the RBC (shown in Fig. 2) vary from 4.5 to 10.5 μm, 1.5 to 3 μm and 0.4 to 0.8, respectively. In this framework, two inverse problems are solved using non-linear regression and identification methods; the first derives the three most important geometrical properties R_1, R_2, R_3 of the RBC as shown in Fig.2, and the second detects the RBC type from a finite set of RBC alternatives.

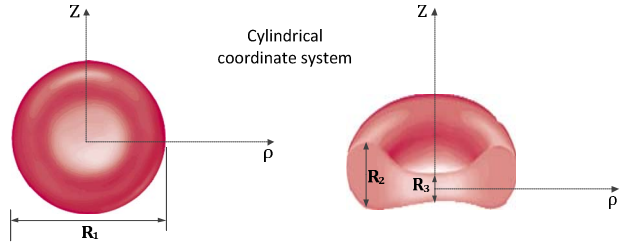

Fig. 2. A representation of a healthy human RBC according to [16,17].

Both solutions share the same processing steps: Image normalization, feature extraction, feature dimensionality reduction of feature vector and feature fusion. In the regression problem, the last processing module consists of a three output RBF-NN where the three geometrical properties are estimated. In the identification problem, the same type of RBF-NN is used and the number of output neurons is equal to the number of RBC types. The identified RBC type is located in the most activated output neuron.

A. *Image Normalization – Feature Extraction*

Taking into account that the mean image brightness is not related to the RBC size, a linear normalization of the pixel intensity values, according to actual mean brightest of the acquired image, is applied to eliminate this irrelevant information. The extraction of the most effective scattering information, which is directly related to the RBC geometrical properties, is close related to the features selection problem. In the absence of related studies, robust feature sets related to the Histogram of Oriented Gradients (HoG) and Region Covariance features (RCoV) are used to encode the image data. The proposed feature extraction, feature dimension reduction and feature fusion process are shown in Fig. 3.

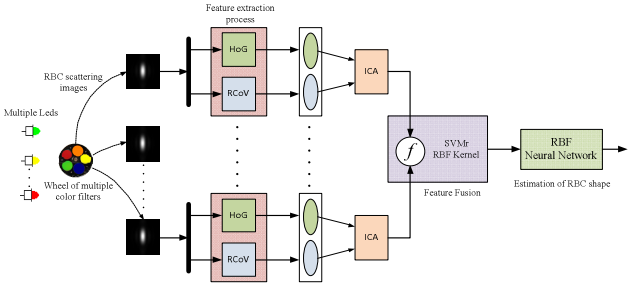

Fig. 3. The feature extraction and feature fusion process.

B. *Histogram of Oriented Gradients*

The HoG [18] is very effective to represent objects and is widely used in human and face detection. Object shape detection is obtained using the distribution of local intensity gradients or edge direction. Initially, the points of interest (PoIs) are determined using the Harris detector and thereafter the HoG is applying at each PoI in the local region of 32×16. The HoG features are estimated by taking the orientation histograms of edge intensity in the local region. Sobel filters are used to obtain the edge gradients and orientations. The gradient magnitude $G(x,y)$ and the orientation $\theta(x,y)$ are estimated using the directional gradients $d_x(x,y)$ and $d_y(x,y)$ computed by Sobel filter:

$$G(x,y)=\sqrt{d_x(x,y)^2+d_y(x,y)^2}$$

$$\theta(x,y)=\begin{cases}\tan^{-1}\left(\dfrac{d_y(x,y)}{d_x(x,y)}\right)-\pi, & d_x(x,y)<0 \wedge d_y(x,y)<0\\ \tan^{-1}\left(\dfrac{d_y(x,y)}{d_x(x,y)}\right)+\pi, & d_x(x,y)<0 \wedge d_y(x,y)>0\\ \tan^{-1}\left(\dfrac{d_y(x,y)}{d_x(x,y)}\right), & \text{elsewhere}\end{cases} \quad (1)$$

The local region is divided in 4×4 sub-region, for each sub-region the 8-bin gradient orientation are estimated which forms a feature vector of size 128 dimension $(4 \times 4 \times 8)$.

C. *Region Covariance Features*

Tuzel, et al. [19,20] have proposed region covariance in the context of object detection. If $\mathbf{I}_s$ is a scattering image and z_p the corresponding feature vector estimated for each pixel of $\mathbf{I}_s$,

$$z_p=\left[x \quad y \quad |I_x| \quad |I_y| \quad \sqrt{I_x^2+I_y^2} \quad |I_{xx}| \quad |I_{yy}| \quad \tan^{-1}\frac{|I_y|}{|I_x|}\right]^T \quad (2)$$

where x and y are the pixel p coordinates, I_x and I_y are the first order intensity derivatives regarding to x and y respectively, I_{xx} and I_{yy} are the second order derivatives, and the last term of eq.2 is the edge orientation. The feature vector z_p is estimated using the same PoIs where HoG is applied. For each local region of $\mathbf{I}_s$ the covariance matrix C_R expressed:

$$C_R=\frac{1}{N-1}\sum_{p=1}^{N}(z_p-\bar{\mu})\cdot(z_p-\bar{\mu})^T \quad (3)$$

where $\bar{\mu}$ is the mean value of z_p over the local region while N is the total number of pixels of the region. The size of the covariance matrix C_R is 8×8; and due to symmetry of C_R only its lower triangular part need to be used. Hence, the feature vector of the local region consists of 36 coefficients.

D. *Features Reduction*

The feature extraction method must be effectively extract, eliminate redundancy and compress the scattering information related to the RBC size from the acquired images. The elimination of the information redundancy is achieved using the well-known ICA [21-23], applied on

linearly mixtures sources in the feature space. The features reduction process is obtained in the new linearly transformed space by selecting the features with large eigenvalues.

E. Features Fusion

A scheme using support vectors machine (SVMr) [24] for regression is adopted in order to fuse the multimodal features. Since this work treats a large dataset, the Radial Basis Function (RBF) kernel has been chosen, due to its suitable computational cost. When using SVM with linear or polynomial kernels, the margin parameter C cannot be sufficiently adjusted. The parameter C determines the trade-off between maximization of the margin and minimization of the classification error. In SVM regression, the input $\mathbf{x}$ is mapped onto a n-feature space using a nonlinear mapping, and then a linear model is constructed (eq. 4) in this feature space:

$$f(\mathbf{x},\omega)=\sum_{i=1}^{n}\omega_i\cdot g_i(\mathbf{x})+b\,, \tag{4}$$

where $g_i(\mathbf{x})$, $i=1,\cdots,n$, denotes a set of nonlinear transformations, and b is the bias term.

F. Estimation of RBC Shape using the RBF-NN

Artificial neural networks have been used widely in many non-linear regression and classification problems [25-28] using computing elements, simulating the information processing of biological neurons. The popular RBF-NN has very efficient training algorithms and only the number of hidden neurons must be defined by the network designer. In the proposed method, the fused feature vector obtained by the SVM scheme is non-linearly processed by the RBF-NN to derive the actual RBC size as in [29]. The radius of the adopted radial-basis functions, denoted as spread, can be a network or neuron dependent parameter or can be estimated as part of the training process [27].

III. Numerical Experimental Results

A database of 3 Leds × 5 filters × 1575 RBCs = 23625 images of 50 × 50 pixels size each is developed. The image database has been designed to cover the RBCs typical size in equal steps of 0.250 μm for R_1 and R_2 and 0.05 for the ratio $\frac{R_3}{R_2}$. In regression experiments, the geometrical properties of RBCs are estimated from the set of scattering images simulating the proposed device. In identification numerical experiments, each set of scattering images is classified into a valid set of 787 unique RBC geometry configurations. The simulated images are estimated using, the spectral responses of three LEDs, the five optical color filters and the solution of the scattering problem of a monochromatic EM plane wave, taking into account both axisymmetric geometry of the scatterer and the non-axisymmetric boundary conditions. Multiple wavelength scattering images are derived using the boundary element method (BEM) developed in [5].

A. Training and Evaluation of the RBF-NN

The original images are distorted using both additive white Gaussian noise from 60 to 10 dB SNR which approximate several phenomena in real image acquisition systems (such as thermal-noise in CCD) and systematic distortions which caused by non-proper alignment of optical and sensor elements. The training data of the RBF-NN consist of 788 RBC configurations, i.e. 3 LEDs × 5 color filters × 788 RBCs = 11820 images are used, and for the regression and identification numerical experiments the remaining 11805 images are selected. Both training and testing sets are uniformly distributed in the RBC sizes. The identification process is completed by the nearest classification rule of the Euclidean distance between the regression values estimated by RBF-NN and the actual 787 RBC sizes used to build the image database. In the hidden layer of the RBF-NN, both the number of neurons and the spread value of the Gaussian radial function kept constant with values 100 and 10 respectively. In the regression numerical experiments the features derived by the histogram oriented gradients and region covariance are trainable fused by the SVM scheme. In the evaluation process the mean absolute error between the actual geometrical properties of the RBC and the RBF-NN is estimated, denoted as regression error (MRE). As shown in Fig. 4, the geometrical parameters of RBC have an optimal estimation with MREs less than of 2% at 30 dB SNR respectively.

The mean identification rate (MIR) versus the level of noise is estimated giving mean error of the estimated geometrical parameters of erythrocyte less than 1% of the actual RBC size when the signal to noise ratio is greater than 60 dB. A quantitative comparison of the method accuracy is given in Fig.5 where the MIR is compared with the rate achieved at [12]. The proposed method, gives best results with remarkable robustness in the noise presence. At 10 dB SNR the mean identification rate exceeds to 80%.

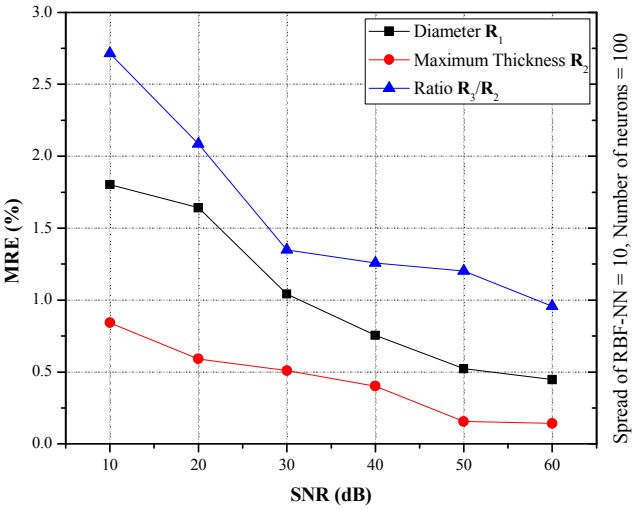

Fig. 4. The mean regression error versus the noise level.

In order to visualize the classifier's performance in Fig. 6 a ROC curve, is presented. An ROC graph depicts relative tradeoffs between benefits (true positives) and costs (false

positives) for different values of parameter R_1, R_2 and $\frac{R_3}{R_2}$. As it is shown, the closer the curve follows the left-hand border and then the top border of the ROC space, the more accurate the classification result which is achieved, as expected.

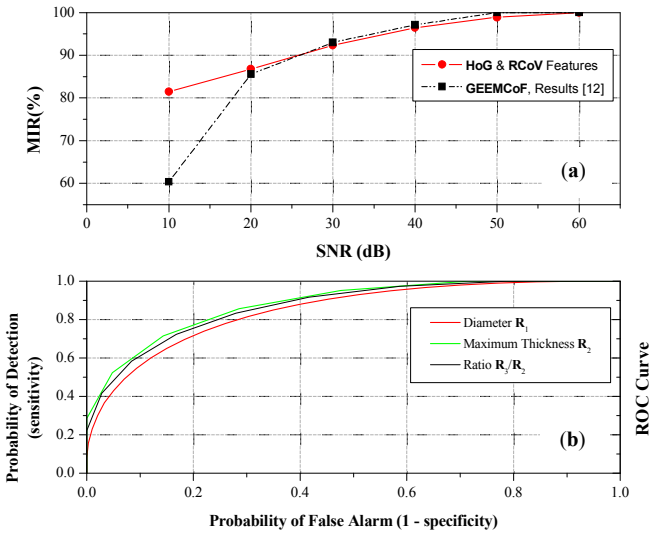

Fig. 5. (a) The mean identification rate versus the noise level (b) the ROC curve.

IV. Conclusion

In this paper, a fully automated method for the estimation of RBC shape using image processing and supervised neural network techniques are implemented and numerical evaluated. The scattering phenomena of a RBC are recorded in images whereas each image is acquired using a unique pair of LED and color filter. As shown in the section 3, excellent detection and identification rates for three important geometrical properties of human biconcave-shaped RBC are obtained by the proposed method, even in cases where the simulated images are distorted by white Gaussian noise at the very noisy environment of 10 dB SNR. The excellent performance of the proposed method remains even in case of additive noise providing an important guideline for medical implementation in real-life applications. The proposed method can be extended both to identify and estimate the distribution other type of microparticles using multiple scattered light images.

References

[1] V. Twersky, "Absorption and multiple scattering by biological suspensions", Journal of Optical Society America A 8 (1991) 1135–1141.

[2] J. Kim, J.C. Lin, "Successive order scattering transport approximation for laser light propagation in whole blood medium", IEEE Transactions of Biomedical Engineering 45 (1998) 505–510.

[3] A.H. Gandjbakhche, P. Mills, P. Snarbe, "Light-scattering technique for the study of orientation and deformation of red blood cells in a concentrated suspension", Applied Optics 33 (1994) 1070–1078.

[4] G.N. Constantinides, D. Gintides, S.E. Kattis, K. Kiriaki, C.A. Paraskeya, A.C. Payatakes, D. Polyzos, S.V. Tsinopoulos, S.N. Yannopoulos, "Computation of light scattering by axisymmetric nonspherical particles and comparison with experimental results", Applied Optics 37 (1998) 7310–7319.

[5] S.V. Tsinopoulos, D. Polyzos, "Scattering of He–Ne laser light by an average-sized red blood cell", Applied Optics 25 (1999) 5499.

[6] M. Kinnunen, A. Kauppila, A. Karmenyan, R. Myllyla, "Effect of the size and shape of a red blood cell on elastic light scattering properties at the single-cell", OSA, Biomedical Optics Express 2 (2011) 1803–1814.

[7] D. Strokotov, A.E. Moskalensky, V.M. Nekrasov, V.P. Maltsev, "Polarized lightscattering profile-advanced characterization of nonspherical particles with scanning flow cytometry", Journal of International Society for Advancement of Cytometry, Part A (2011) 570–579.

[8] L. Golan, D. Yelin, "Flow cytometry using spectrally encoded confocal microscopy", Optics Letters 35 (2010) 2218–2220.

[9] H. Ding, Z. Wang, F. Nguyen, S.A. Boppart, L.J. Millet, M.U. Gillette, J. Liu, M. Boppart, G. Popescu, "Fourier transform light scattering (FTLS) of cells and tissues", Journal of Computational and Theoretical Nanoscience 7 (2010) 1–11.

[10] J.A. Dharmadhikari, D. Mathur, "Using an optical trap to fold and align single red blood cells", Current Science 86 (2004) 1432–1437.

[11] P.J. David, A.C. Nair, V.J. Menon, D.N. Tripathi, "Laser light scattering studies from blood platelets and their aggregates", Colloids and Surfaces B: Biointerfaces 6 (1996) 101–114.

[12] G. Apostolopoulos, S. Tsinopoulos and E. Dermatas, "A methodology for estimating the shape of biconcave red blood cells using multicolor scattering images", Journal of Biomedical Signal Processing and Control, Elsevier, 8 (2013) pp. 263-272.

[13] C. Harris and M.J. Stephens. "A combined corner and edge detector". In Proc. Alvey Vision Conference, pp.147-152, 1988.

[14] K. Mikolajczyk and C. Schmid. "An affine invariant interest point detector" in Proc. of the 7th European Conf. on Computer Vision. Copenhagen, Denmark, vol. I, pp. 128–142. 2002.

[15] D. Lowe. "Object Recognition from Local Scale-Invariant Features", in Proc. of the 7th Int. Conf. on Computer Vision. vol. 2, p. 1150. September 20–25, 1999. IEEE, 1999.

[16] P.W. Kuchel, E.D. Fackerell, "Parametric equation representation of biconcave erythrocytes", Bulletin of Mathematical Biology 61 (1992) 209–220.

[17] S. Munoz San Martin, J.L., Sebastian, M. Sanchol, G. Alavarez, "Modeling Human Erythrocytes shape and size abnormalities", q-bio. QM/0507024, 2005.

[18] N. Dalal and B. Triggs. "Histograms of oriented gradients for human detection", in CVPR (1), pages 886–893, 2005.

[19] O. Tuzel, F. Porikli, and P. Meer, "Human detection via classification on Riemannian manifolds," in Proc. IEEE Conf. Comp. Vis. Patt. Recogn., Minneapolis, MN, 2007.

[20] O. Tuzel, F. Porikli, and P. Meer, "Region covariance: A fast descriptor for detection and classification," in Proc. Eur. Conf. Comp. Vis., Graz, Austria, May 2006, vol. 2, pp. 589–600.

[21] A. J. Bell, T. J. Sejnowski, "An information-maximization approach to blind separation and blind deconvolution", Neural Comp. Vol. 7, pp. 1129–1159, 1995.

[22] P. O. Hoyer and A. Hyvarinen, "Independent component analysis applied to feature extraction from colour and stereo images", Network: Computation in Neural Systems 11(3), pp. 191-210, 2000.

[23] A. Hyvarinen, "Fast and robust fixed point algorithms for independent components analysis", IEEE Trans. Neural Networks 10(3), pp. 626-634, 1999.

[24] V. N. Vapnik, "Statistical Learning Theory", John Wiley and Sons, 1998.

[25] L. Song an F. Arman and J. A. Pearce, "Unsupervised classification of cell images using pyramid node linking", IEEE Trans. BME (37) 6: 647-652, 1990.

[26] J. Park I.W. Sandberg, "Universal approximation using radial basis functions networks", Neural Comput. 5, 305-316, 1993.

[27] D. Wettschereck and T. Dietrich, "Improving the performance of radial basis function networks by learning center locations", In Advances in Neural Information Processing Systems, Morgan Kaufman Publishers, Vol. 4, pp. 1133-1140, 1992.

[28] M. J. Orr, "Regularization in the selection of radial basis function centers", Neural Comput., Vol 7, pp. 606-623, 1995.

[29] A. K. Jain and R. C. Dubes, "Algorithms for Clustering Data", Prentice Hall, NJ, 1988.